

Isostructural phase transition and equation of state of type-I and type-VIII metallic sodium borosilicide clathrates

M. Demoucron^{1*}, S. Pandolfi¹, Y. Guarnelli¹, B. Baptiste¹, P. Chevignon², N. Guignot², D. Portehault³, T.A. Strobel⁴, W.A. Crichton⁵, Y. Le Godec^{1*}, and A. Courac^{1*}

¹ Sorbonne Université, MNHN, UMR CNRS 7590, IMPMC, 75005 Paris, France.

² Synchrotron SOLEIL, 91192 Saint Aubin, France.

³ LCMCP, Sorbonne Université, UMR CNRS 7574, 75005 Paris, France.

⁴ Geophysical Laboratory, Carnegie Institution of Washington, Washington, DC 20015, USA. and

⁵ ESRF, The European Synchrotron, Grenoble, France.

(Dated: December 5, 2025)

Electronic properties of silicon-based clathrates can be tuned by boron incorporation into the silicon cage network. Sodium borosilicides clathrate outstands with uncommon stoichiometry and expected metallic properties, in contrast to other alkali metal semiconductive Zintl borosilicides. In this study, we report an experimental investigation of the high-pressure behavior of type-I and type-VIII sodium borosilicide clathrates. An isostructural phase transition, marked by an abrupt volume collapse at 13 GPa, is observed exclusively in type-I sodium borosilicide clathrates. This transition is attributed to the pressure-induced diffusion of silicon atoms into cationic sites. This mechanism provides the first experimental validation of a transition predicted theoretically for this class of materials. Isostructural phase transitions were only observed in type-I borosilicide. In contrast, the type-VIII borosilicide phase exhibits conventional elastic compression. The metallic character was established using reflectance spectroscopy over a wide energy range, in good agreement with crystallographic data on the boron content.

Silicon intermetallic clathrates are cage-like framework materials that hold great promise for applications in photovoltaics [1, 2], superconductivity [3], batteries [4] and gas storage [5]. For a relatively small number of crystallographic structures (zeolite-type), a wide range of chemical compositions is possible. Most reported clathrates crystallize in the cubic type-I structure ($Pm\bar{3}n$ space group), which consist of an arrangement of two small 5^{12} cages (dodecahedron, 12 pentagonal faces) and six larger $5^{12}6^2$ cages (tetrakaidekahedron, 12 pentagonal faces and 2 hexagonal faces) [6]. On the other hand, only a few compounds with a type-VIII structure ($I\bar{4}3m$ space group) exist. It features an alternative polyhedral arrangement in a body-centered cubic structure made of uncommon asymmetric cages with 20+3 vertices/atoms [7]. Due to the asymmetry of type-VIII clathrate cages, small cavities surrounded by eight atoms are also part of the structure [8]. In both structure types, the cages are occupied by electropositive guest atoms that donate their electrons to the covalent silicon-based framework.

The conditions for the formation of type-VIII silicon clathrates are still unexplained and no binary M_8Si_{46} ($M = Na, K$ or Ba) compounds having the type-VIII structure have ever been reported. All known type-VIII clathrates require the incorporation of additional group-13 elements. Also, compounds with identical stoichiometry that crystallize in both type-I and type-VIII frameworks are rare; a notable example is the borosilicide $Na_8B_4Si_{42}$ clathrate, which has been reported in both

structural types [9]. In these clathrates, alkali metals donate electrons to compensate for the octet-rule deficiency induced by boron substitution for silicon inside the four-bonded atom framework. In the type-I model structure, boron atoms substitute silicon within the $16i$ and $24k$ Wyckoff sites (See Figure 1.a). In the type-VIII structure, boron atoms substitute silicon at the $8i$ site (See Figure 1.d). In this work, we studied a series of ternary Na–B–Si compounds under high-pressure, high-temperature conditions, four type-I and a unique type-VIII borosilicide clathrates. We investigated their behavior under high quasi-hydrostatic pressure and revealed an isostructural phase transition driven by the pressure-induced diffusion of silicon into the cationic sites.

With one exception [10], the synthesis of boron-doped silicon clathrates requires the application of high pressure, as demonstrated for $Rb_8B_8Si_{38}$ [11], $Cs_8B_8Si_{38}$ [12] and $Na_8B_4Si_{42}$ [9]. Compression promotes inter-diffusion and partial substitution of silicon by boron, thereby tuning the band-gap energy and strengthening the covalent intermetallic framework. Consequently, our borosilicide clathrates samples were synthesized using large volume multi-anvil presses in order to reach moderate pressure below 4 GPa. Type-I $Na_8B_xSi_{46-x}$ samples were obtained at 3.5 GPa and 1150 K, whereas the stoichiometric $Na_8B_{4.1(1)}Si_{41.9(1)}$ sample was produced at higher pressure and temperature (4 GPa and 1500 K). Finally, a boron-free type-I Na_8Si_{46} clathrate was synthesized via a conventional route as a reference sample [13]. All the details of these procedures are described in the Supplementary Material. The boron content of all synthesized samples and the associated bulk moduli and pressure derivatives discussed below are summarized in Table I.

* martin.demoucron@sorbonne-universite.fr,
yann.le.godec@sorbonne-universite.fr,
alexandre.courac@sorbonne-universite.fr

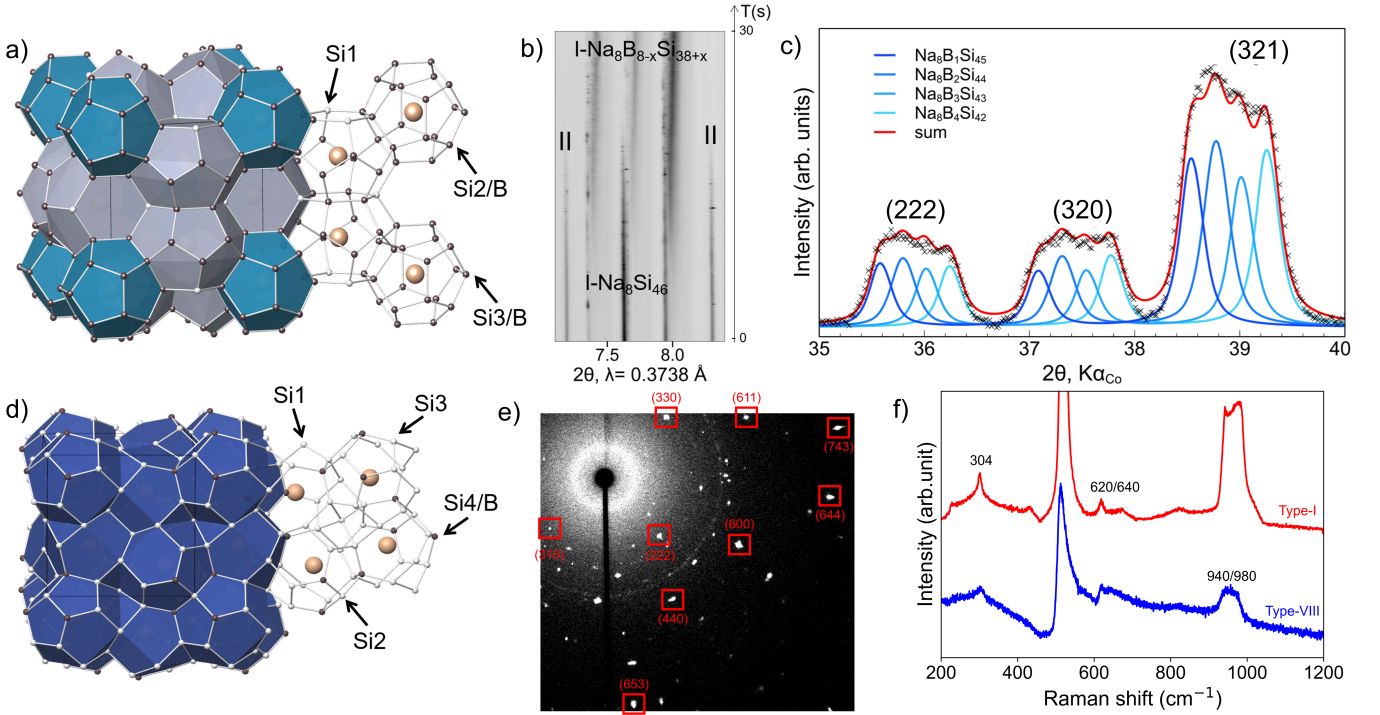


FIG. 1. a) Crystal structure of type-I $\text{Na}_8\text{B}_x\text{Si}_{46-x}$ clathrate. b) Evolution of the *in-situ* XRD diffraction signal (between 7.1 and 8.4°) through high pressure high temperature conditions (large volume press experiment, 1100 K – 3.5 GPa). c) XRD powder pattern (between 35 and 40°) of the sample synthesized at 3.5 GPa and 1150 K, the intensities of the computed phases are calculated from $\text{Na}_8\text{B}_1\text{Si}_{45}$ to $\text{Na}_8\text{B}_4\text{Si}_{42}$ fixed stoichiometry with boron atom inside the 16*i* and 24*k* Wyckoff sites. d) Crystal structure of type-VIII $\text{Na}_8\text{B}_x\text{Si}_{46-x}$ clathrate. e) Part of type-VIII $\text{Na}_8\text{B}_{4.1}\text{Si}_{41.9}$ single-crystal XRD detector image with some indexed reflections. f) Raman spectrum at ambient condition of type-I borosilicide powder sample and $\text{Na}_8\text{B}_{4.1}\text{Si}_{41.9}$ type-VIII single-crystal clathrate.

Composition	Synthesis conditions	a_0 (Å)	Equation of state			Reference
			P_{range} (GPa)	B_0 (GPa)	B_0'	
$\text{Na}_8\text{Si}_{46}$ - type-I	See text	10.200(1)*	[0-20]	64.7(18)	6.8(5)	This work
$\text{Na}_8\text{B}_{4.8}\text{Si}_{41.2}$ - type-I		9.936(14)	[0-13]	86.6(17)	2.5(3)	This work
$\text{Na}_8\text{B}_{3.7}\text{Si}_{42.3}$ - type-I	3.5 GPa/1150 K	9.999(5)	[0-13]	99(5)	1.5(8)	This work
$\text{Na}_8\text{B}_{2.9}\text{Si}_{43.1}$ - type-I		10.041(2)	[0-12]	88(11)	3.7(18)	This work
$\text{Na}_8\text{B}_{4.1(1)}\text{Si}_{41.9(1)}$ - type-VIII	4 GPa/1500 K	9.699(1)*	[0-22]	90.2(13)	3.8(2)	This work
$\text{Na}_8\text{B}_{4.1(7)}\text{Si}_{41.9(7)}$ - type-I	5 GPa/1200 K	9.977(1)	-	-	-	[9]
$\text{Na}_8\text{B}_{4.2(1)}\text{Si}_{41.8(1)}$ - type-VIII	6 GPa/1200 K	9.7187(2)	-	-	-	[9]

TABLE I. Sample properties and P-V equation of state data (2nd order *Vinet* EoS was used [14]). *: fixed a_0 from powder XRD at ambient conditions.

The *in-situ* high-pressure high-temperature XRD measurements at 1100 K (See Figure 1.b) reveal the emergence of spots corresponding to individual type-I clathrates with reduced lattice parameters. Type-I borosilicide clathrates formed at the expense of the boron-free $\text{Na}_8\text{Si}_{46}$ (type-I) and $\text{Na}_{24}\text{Si}_{136}$ (type-II) clathrates as respectively identified in references [15] and [16]. The associated *ex-situ* XRD of the recovered sample is represented on Figure 1.c and reveals a wide range of boron content within type-I $\text{Na}_8\text{B}_x\text{Si}_{46-x}$ clathrates at ambient conditions. The broadening of powder XRD

reflections indicates a mixture of compounds or solid solutions with various boron concentrations, rather than a non-homogeneous boron distribution within one phase, with local regions exhibiting lattice parameters ranging from 10.147 down to 9.973 Å—in contrast with the Si-Ge system and other solid-solutions [17]. The significant volume reduction compared to the boron-free type-I $\text{Na}_8\text{Si}_{46}$ clathrate ($a_0=10.2004(3)$ Å) provides unambiguous evidence of the presence of boron within the structure [18] as it was observed under extreme conditions. Le Bail refinement of the *ex-situ* XRD pattern was per-

formed using four phases, with boron atoms occupying the $16i$ and $24k$ Wyckoff sites. By default, four phases were used to describe the XRD signal, but the number of phases within this sample is unknown and could encompass more components. Nonetheless, at high 2θ angles, where many peaks overlap, the calculated $\text{Na}_8\text{B}_x\text{Si}_{46-x}$ phases accurately reproduce the XRD signal (see Supplementary Material, Figure S2 [19]), thereby confirming the validity of the fit. Nonhomogeneous boron distribution was already suggested by *Jung et al.* [10, 20] in the K-B-Si system. Distinct phases with different boron contents ($\text{K}_{8-x}\text{B}_y\text{Si}_{46-y}$) describe the same continuous range of boron content within the type-I clathrate. Each measured composition (from $\text{K}_{6.80(2)}\text{B}_{6.4(5)}\text{Si}_{39.6(5)}$ to $\text{K}_{7.85(2)}\text{B}_{7.8(1)}\text{Si}_{38.2(1)}$) corresponds to a distinct lattice parameter. On the other hand, synthesis under higher pressure and temperature conditions stabilizes this unique type-VIII borosilicide phase, along with two other distinct type-I borosilicide clathrates. Type-VIII borosilicide clathrate crystals were extracted from powder to conduct single-crystal XRD under ambient conditions. Single-crystal XRD signal (See Figure 1.e) clearly shows the existence of a single phase with a structure and a composition similar to that previously reported [9]. Raman spectroscopy at ambient conditions (See Figure 1.f) was also performed on the same crystal. A similar Fano profile and anti-resonance dip from low-energy side is observed in heavily doped p-type silicon around 512 cm^{-1} [21]. This asymmetric line shape appears exclusively in the type-VIII clathrate, in agreement with a metallic character [22]. The band near $620/640\text{ cm}^{-1}$ serves as a fingerprint of boron incorporation in the silicon network [21]. High-temperature Raman spectroscopy confirmed the thermal stability of this single-crystal up to 1273 K (see Supplementary Material, Figure S6 [19]), while Fano feature is clearly observed up to 873 K . FTIR spectroscopy was further performed on the same $\text{Na}_8\text{B}_{4.1}\text{Si}_{41.9}$ type-VIII single-crystal in both the near- ($500\text{--}7000\text{ cm}^{-1}$) and mid-IR ($8500\text{--}22500\text{ cm}^{-1}$) ranges (See Supplementary Material, Figure S7 [19]). The reflectance spectra display a metallic response, similar to that of gold or aluminum, with comparable trend [23]. No transmission is observed in either spectral range, consistent with metallic behavior, in contrast with narrow bandgap like BC8 silicon [24].

The Zintl-Klemm concept [25] would predict a $\text{Na}_x\text{B}_x\text{Si}_{46-x}$ composition for both clathrate types, but according to previously reported stoichiometry [9] and our type-VIII single-crystal XRD measurement (discussed later), the $\text{Na}_8\text{B}_x\text{Si}_{46-x}$ stoichiometry is retained for all samples. The boron concentration in each clathrate cannot be determined by our powder XRD data, therefore, we assume that the sodium borosilicide crystals obey *Vegard's law* [26], previously validated for $\text{K}_{8-x}\text{B}_y\text{Si}_{46-y}$ type-I clathrates [20], which describes a linear relationship between the lattice parameter and the boron content. Using the previously reported sodium borosilicide lattice parameter [9], we evaluate the boron

contents of the three type-I borosilicide clathrates identified in the sample as 2.9, 3.7 and 3.8 at.% (See Supplementary Material, Figure S3 [19]). Type-VIII borosilicide clathrate single crystals could be extracted from the crushed sample synthesized at 4 GPa and 1500 K and subsequent single crystal XRD analyses were performed. The refined stoichiometries and the lattice parameters are found to be very close to the structure reported by *Hübner et al.* [9]. Boron atoms substitute silicon only in the $8c$ Wyckoff site and no residual boron was found into other sites. Furthermore, a significant electron density has been identified at the center of the cages. By setting the number of sodium atoms at a value of one per cage, both the $\text{Na}_8\text{B}_{4.1(2)}\text{Si}_{41.9(2)}$ and $\text{Na}_8\text{B}_{4.51(10)}\text{Si}_{41.49(10)}$ stoichiometries are calculated on two different samples (See Supplementary Material Tab. S1 - Tab. S3 [19]).

The behavior under pressure of type-I and type-VIII borosilicide clathrates was studied in order to probe their previously unknown elastic properties and reveal isostructural phase transitions. The samples were loaded into diamond anvil cells (DACs) equipped with $400\text{ }\mu\text{m}$ culet diamonds to reach 20 GPa. $40\text{ }\mu\text{m}$ thick rhenium gaskets with a $150\text{ }\mu\text{m}$ diameter hole were used and filled with neon or argon gas as pressure-transmitting media. The increase of pressure was achieved by a gas membrane. A small amount of gold powder was placed as a pressure calibrant inside each DAC. *In-situ* XRD analyses were carried out at synchrotron SOLEIL on the PSICHÉ beamline with a beam wavelength of 0.3738 \AA . The beam size was approximately $10 \times 10\text{ }\mu\text{m}$, while the sample measured around $50\text{ }\mu\text{m} \times 50\text{ }\mu\text{m} \times 20\text{ }\mu\text{m}$. This *in-situ* characterization enabled us to follow the lattice evolution and determine the equation of state (EoS) of compounds from precise Rietveld refinements with $0.01^\circ\text{ }2\theta$ resolution. The boron-free $\text{Na}_8\text{Si}_{46}$ clathrate exhibited a powdered diffraction signal, whereas the type-I and type-VIII borosilicide clathrates produced spotty diffraction patterns, typically showing 5 to 15 intense spots per ring. Nevertheless, this was sufficient for diffractogram integration. To obtain accurate pressure values, XRD patterns of gold were acquired before and after measuring sample, and the average gold cell volume was used as a pressure gauge. The Anderson EoS of gold [27] was employed to determine the pressure at each experimental point. Rietveld refinements were performed using the MAUD software [28] to extract both sample and pressure calibrants lattice parameters. Additional pressure calibrants with known EoS, including cubic silicon [29], solid neon [30], and solid argon [31] were also used.

Synchrotron XRD patterns were recorded over a pressure of $\sim 0.5\text{ GPa}$ to 20 GPa at 300 K. The initial XRD patterns of the compounds, collected from different regions of the cell, are shown in Figure S4 of the Supplementary Material. The presence of elemental cubic silicon-I inside the sample synthesized at 3.5 GPa and 1150 K, likely results from incomplete reaction during clathrate formation. When silicon was detected, the cubic-to-hexagonal phase transition ($\text{Si-I} \rightarrow \text{Si-V}$) oc-

curred at 13 GPa, while the intermediate tetragonal and orthorhombic phases (Si-II and Si-XI) were not always observed. A trace amount of rhenium, used as a DAC gasket, is also discernible through the observation of minor and broad peaks situated around $Q = 2.9 \text{ \AA}^{-1}$. The small beam size limited the number of grains probed, resulting in texture on the 2D image detector and deviations of peak intensities from theoretical ratios. However, the presence of type-I and type-VIII clathrate phases was clearly identified.

Figure 2.a shows the pressure-volume (P-V) experimental data for all clathrate samples up to 22 GPa, along with a picture of one DAC loading. In three different static compression experiments, four distinct type-I clathrate phases were investigated: one sodium silicide and three Na-B-Si phases. All phases exhibit simultaneous volume reduction without any crossover between their P-V curves. The data are continuous up to 13 GPa and fit well to the Vinet EoS. Above 13 GPa, only $\text{Na}_8\text{Si}_{46}$ exhibits a continuous compression behavior, whereas the three type-I borosilicide clathrates phases display a sudden volume collapse near 13 GPa. This phenomenon was reproducible in two different DAC experiments. Neon, used as a pressure-transmitting medium, solidifies above 4 GPa and thereafter serves as a pressure gauge. The Si-I phase is observed below 13 GPa, prior to the Si-I \rightarrow Si-V phase transition. Those pressure gauges, Si [29], Ne [30] and Ar [31] are essential to testify the possible stress over the cell arising during transformations by comparison to the gold gauge. They confirm that the observed volume collapse is not due to any pressure calibration error. The extracted pressure values from all calibrants are compared with those obtained from gold (See Supplementary Material, Figure S5 [19]).

The volume collapse at 13 GPa is observed without any change in crystal symmetry (See Figure 2.b). Analysis of the XRD patterns during compression shows that the shape and position of each diffraction spot remain nearly unchanged across the transition, even after the volume collapse. The volume collapse is therefore attributed to an isostructural phase transition, similar to those previously observed for in K-Si and Ba-Si type-I clathrates [32–35]. The theoretical study of *Itaka* [36] suggests a possible mechanism of this isostructural phase transition, which starts with the creation of Si vacancies under high pressure, especially at the $6c$ silicon site. In this mechanism, free silicon atoms can diffuse and form silicon-rich phases such as B-doped diamond-like silicon, at the grain boundaries. This transition is driven by the diffusion of Si atoms into vacant cation sites at higher pressure. Because only a limited number of hkl reflections (≤ 8) were available for refinement, only two site occupancy factors (SOFs) could be refined simultaneously to ensure reliable and meaningful results. Figure 3.a shows the refined SOFs for silicon ($16i$) and sodium ($6d$) sites. Some SOFs values above unity can be attributed by spotty diffraction patterns, leading to an incorrect evaluation of peak intensities. However, the

trends of SOFs after 13 GPa show clear transitions and especially the increase of occupancy for the Na-site correlated with a decrease of the occupancy of Si in the tetrahedral framework. This indicates the diffusion of silicon atoms into the cage sites. This isostructural transition induces microstrain within the sample due to cage rearrangement (See Figure 3.b). At low pressure, prior to Ne solidification, both the SOFs and microstrain exhibit anomalous behavior, likely arising from diffuse scattering of the gas pressure-transmitting medium. Overall, the evolution of cell volume, site occupancies, and microstrain supports the mechanism proposed by *Itaka* [36], in which silicon atoms migrate from the tetrahedral covalent framework to the cage sites. The observed sudden change of compressibility could be thus explained by the formation of Si/B vacancies within the cage framework. The same isostructural phase transition phenomena was not observed in the boron-free $\text{Na}_8\text{Si}_{46}$ type-I clathrate and within the $\text{Na}_8\text{B}_{4.1(1)}\text{Si}_{41.9(1)}$ type-VIII clathrate (See Figure 2.c). This can be explained by a lack of vacancies within these two stoichiometric compounds. According to the single crystal data analysis of the type-VIII $\text{Na}_8\text{B}_{4.1(1)}\text{Si}_{41.9(1)}$ clathrate, all the cages are fully occupied, thus, any volume collapse is observed up to 20 GPa.

The values of bulk moduli of three observed borosilicides type-I clathrate phases were then calculated from the P-V curves at pressures below the isostructural phase transition, i.e. for the 0-13 GPa range. All data were fitted using the third-order Vinet equation of state implemented in the EoSFit7 software [37]. The ambient-pressure lattice parameters, fitting pressure ranges, and corresponding compressibility parameters are summarized in Table I. For samples with unknown ambient lattice parameters (a_0), these values were left free during fitting. Boron incorporation into the type-I framework increases the bulk modulus. This phenomenon can be attributed to the strong covalent bond between boron and silicon. On the other hand, the type-VIII $\text{Na}_8\text{B}_{4.1}\text{Si}_{41.9}$ clathrate exhibits a lower lattice parameter in comparison to all type-I clathrates, and 10.7 % higher crystallographic density than the $\text{Na}_8\text{Si}_{46}$ type-I clathrate. Despite this, its bulk modulus is comparable to that of type-I clathrates. The borosilicide clathrates exhibit B_0 values of bulk moduli that fall within the range of d -Si [29, 38]. This fact further corroborates the notion that isolated grains of type-I phases are characterised by distinct properties, thus underscoring the necessity for dedicated research in this area.

Finally, we presented distinct syntheses of boron-free and borosilicide type-I and type-VIII clathrates. Time-resolved *in-situ* XRD enabled us to identify at least three different type-I borosilicide clathrates, which exhibit an abrupt volume collapse above 13 GPa. We attribute this behavior to an isostructural transition driven by atomic migration from the tetrahedral framework into the clathrate cages. In contrast, type-I $\text{Na}_8\text{Si}_{46}$ and type-VIII $\text{Na}_8\text{B}_{4.1}\text{Si}_{41.9}$ clathrates remain structurally

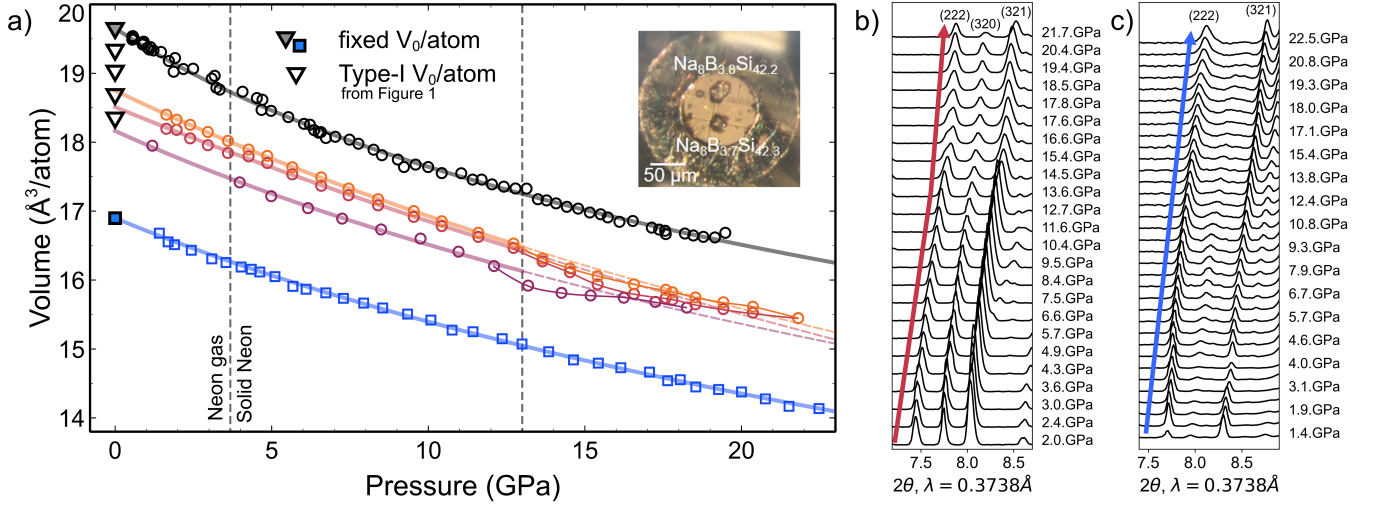


FIG. 2. a) The P-V experimental data and their corresponding Vinet EoS fitting along with the picture of $\text{Na}_8\text{B}_{4.8}\text{Si}_{41.2}$ and $\text{Na}_8\text{B}_{3.7}\text{Si}_{42.3}$ samples inside the DAC. The black curve corresponds to the boron-free type-I $\text{Na}_8\text{Si}_{46}$ clathrate. The blue curve corresponds to the type-VIII $\text{Na}_8\text{B}_{4.1(1)}\text{Si}_{41.9(1)}$ clathrate. All the other samples correspond to the $\text{Na}_8\text{B}_x\text{Si}_{46-x}$ type-I clathrates ranging from orange to purple according to their initial lattice parameter. The initial V_0 volume of the borosilicides type-I clathrates synthesized at 3.5 GPa and 1150 K are unknown and, thus, cannot be fixed during the equations of state fitting. The volume/atom error bars are included in the width of markers. For type-I borosilicide clathrates, above 13 GPa, the solid lines serve as guides to highlight the volume collapse. b) Waterfall plotting of $\text{Na}_8\text{B}_{3.7}\text{Si}_{42.3}$ type-I raw data (222), (320) and (322) XRD triplet. c) Waterfall plotting of $\text{Na}_8\text{B}_{4.2}\text{Si}_{41.8}$ type-VIII raw data (222) and (321) XRD doublet.

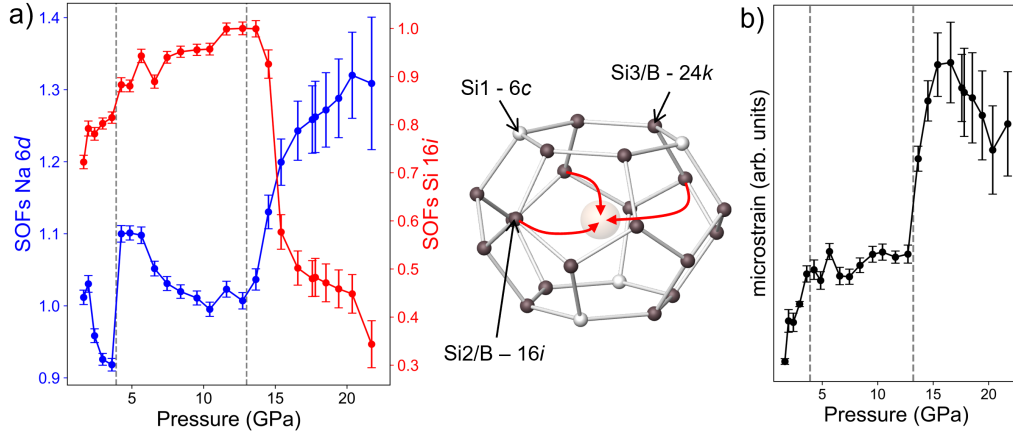


FIG. 3. a) Site-occupancy factors for the 6d and 16i Wyckoff sites with a schematic representation of Si diffusion into the cage center and b) induced microstrain calculated from peaks enlargement.

stable up to 20 GPa. The calculated bulk moduli show a non-monotonous evolution with the boron content or the a_0 lattice parameters. Nonetheless, some bulk modulus measurements were found to be close to those of diamond-like silicon. A type-VIII $\text{Na}_8\text{B}_{4.1}\text{Si}_{41.9}$ clathrate was isolated, and both single crystal XRD, Raman and FTIR spectroscopy (See Supplementary Material [19]) were performed, providing evidence consistent with metallic behavior. The stoichiometry of type-VIII borosilicide clathrates supports the hypothesis that such phases are metallic. At the same time, our attempts to measure electrical resistivity failed due to the inconvenient shape and size of the sample. However, the re-

flectance measurements over a wide photon energy range can help in such a situation, providing alternative insight into conceptual metallicity, as it was proposed for experimental proof of metallic hydrogen [39]. These results clarify the pressure-driven atomistic mechanisms in borosilicide clathrates and open future works for tuning their electronic and mechanical properties for functional applications.

Data availability statement

The data that support the findings of this article are openly available 10.6084/m9.figshare.30647453 [40]. The gold pressure calibration, *in-situ* XRD for synthesis and the single crystal XRD data can be obtained from the corresponding authors upon request.

ACKNOWLEDGMENTS

We acknowledge assistance from the PSICHE beamline staff of synchrotron SOLEIL (Proposals 20210410-BAG, 20220361-BAG and 20240361-BAG for PSICHE beamline). We acknowledge the European Synchrotron Radiation Facility (ESRF) for material support during beamtime at the ID06-LVP beamline under proposal number CH4896 and we acknowledge M. Mezouar for preliminary results acquired on ID27 beamline under proposal number CH4380. We acknowledge the ANR-FRANCE (French National Research Agency) for the financial support of the BCSi project number ANR-21-CE08-0018. We also thank the support of the high-pressure platform of IMPMC laboratory.

SUPPLEMENTARY MATERIAL

A. Sample synthesis

a. Type-I $\text{Na}_8\text{Si}_{46}$ clathrate

The stoichiometric reference $\text{Na}_8\text{Si}_{46}$ type-I (Si-I) clathrate has been prepared at ambient pressure using a classical but recently improved chemical technique, described in the study of *Song et al.* [13]. Na_4Si_4 (4 mmol) was loaded in a pyrolytic h-BN crucible (ϕ 25 × h 60 mm) previously dried at 673 K under vacuum (10^{-3} mbar) for 10 hours. The crucible was inserted in a bottom-closed quartz tube covered with an h-BN cap prior heating, to maintain a high Na vapor pressure. The tube was heated at 743 K under dynamic vacuum (10^{-3} mbar) for 90 min inside a vertical furnace. After dwelling and cooling down, the quartz tube with the h-BN crucible and its containment were transferred into an argon-filled glove-box without exposure to air, and the powder was stored in inert atmosphere.

b. type-I $\text{Na}_8\text{B}_x\text{Si}_{46-x}$ borosilicide clathrates

In-situ high-pressure high-temperature synthesis at 3.5 GPa and 1150 K of sample composed of type-I borosilicide clathrates was performed using the 20MN Vöggenreiter multi-anvil press at beamline ID06-LVP of the ESRF [41]. For this experiment, a mixture of Na_4Si_4 powder (obtained from the synthesis of reference [13]), amorphous boron powder (Sigma-Aldrich, $\geq 95\%$) and silicon powder (Alfa Aesar, 99.999%) with the Na:B:Si atomic ratio of 8:8:38 was ground in a ceramic mortar for one hour inside a high-purity Ar glovebox and loaded

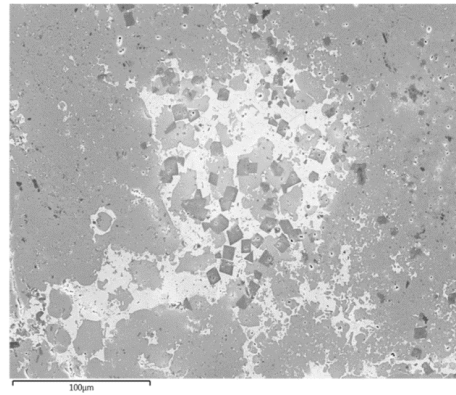


FIG. 4. SEM image with AsB detector of the polished sample synthesized at 4 GPa and 1500 K.

into a h-BN capsule. We used a 14/8 multianvil assembly (MgO octahedron with 14 mm side compressed with eight WC cubic anvils with 8 mm-side triangular truncations), equipped with graphite furnace and alumina cap to achieve 3.5 GPa and 1150 K. Si-I [42] and Na [43] equations of state were used to calibrate pressure and temperature in parallel with estimates based on previous calibration curves [44, 45]. Angle dispersion X-ray diffraction was performed using a wavelength corresponding to 33 keV and collected on an azimuthally-scanning Detection Technology X-Scan c series GOS linear detector. The power was switched off and after that, the pressure was slowly released at the end of the synthesis.

c. type-VIII $\text{Na}_8\text{B}_x\text{Si}_{46-x}$ borosilicide clathrate

A sample made of type-I and type-VIII sodium borosilicide clathrates was obtained from the same mixture described here above. The mixture was compressed into a pellet and then introduced into a similar 18/11 multianvil assembly and compressed to 4 GPa. The heater-sample total resistivity probing method was used to achieve the complete transformation of intermediate metallic clathrates [46]. After the accomplishment of this process, the temperature was gradually decreased over a period of 20 minutes. The latter allowed us to obtain crystallization in (quasi-) equilibrium conditions. The recovered samples were easily removed from the graphite heater. No reaction between the mixture and the graphite capsule or the alumina plugs was detected up to 1500 K at 4 GPa. The type-VIII borosilicide clathrate was found to be the major phase. A small proportion of two type-I clathrate phases were also found inside the same sample powder with $a_0 = 9.9523(9)$ Å and $a_0 = 10.1190(16)$ Å lattice parameters, confirming the presence of boron in their structure.

This mixture of different phase was observed by both XRD and SEM-EDX imaging (See Figure 4). Small polycrystalline grains, as well as clathrate VIII single crystals of approximately 10 μm could be isolated from the grounded mixture [46].

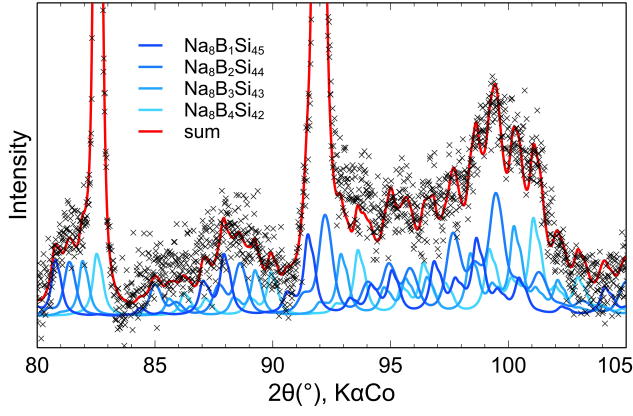


FIG. 5. XRD powder pattern (between 80 and 105°) of the sample synthesized at 3.5 GPa and 1150 K, the intensities of the computed phases are calculated from $\text{Na}_8\text{B}_1\text{Si}_{45}$ to $\text{Na}_8\text{B}_4\text{Si}_{42}$ fixed stoichiometry with boron atom inside the 16i and 24k Wyckoff sites.

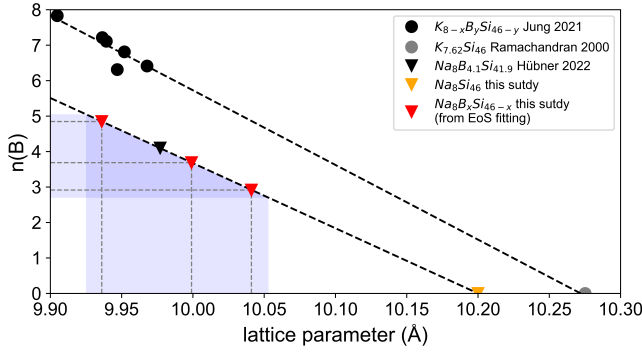


FIG. 6. Boron content of $\text{K}_8\text{B}_x\text{Si}_{46-x}$ and $\text{Na}_8\text{B}_x\text{Si}_{46-x}$ clathrates in function of the lattice parameter. The samples synthesized at 5 GPa and 1150 K were placed from the fitted a_0 lattice parameters from the EoS.

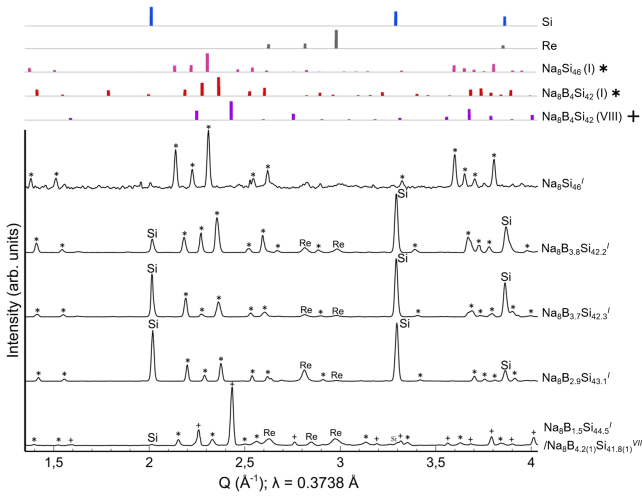


FIG. 7. XRD patterns of every $\text{Na}_8\text{B}_x\text{Si}_{46-x}$ clathrates found at different places in a DAC cell at nearly ambient condition (* : type-I clathrate; + : type-VIII clathrate).

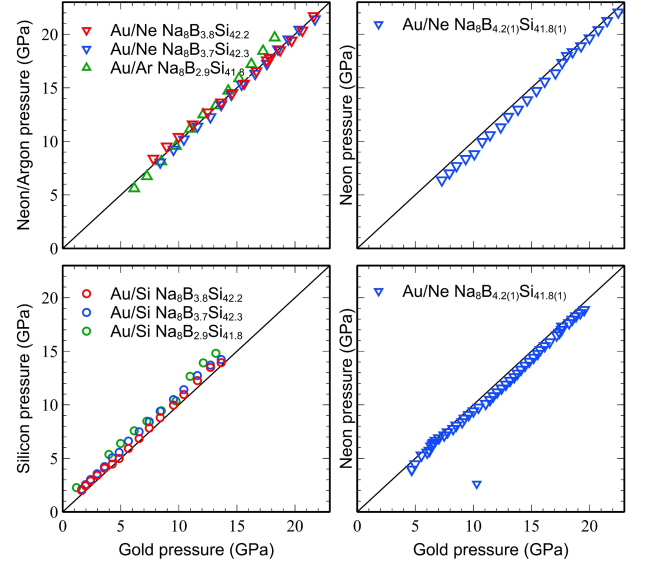


FIG. 8. Comparison between the pressures obtained with gold gauge, pressure medium (Ne or Ar, when solidified) and Si grain of sample. No discontinuity at 13 GPa was observed for the different DAC experiments.

B. Pressure calibration

Since gold and the different samples are not at the same position inside the DAC, the pressure differences between gold and the other pressure calibrants could be explained by the DAC radial pressure gradient [47]. Also, the initial volume of the crystallized neon changes according to various equation of states [30, 48, 49] and could explain the pressure differences between gold and neon. However, no significant disruption is observed around 13 GPa, therefore ensuring the reliability of the pressure calibration.

C. Type-VIII borosilicides clathrates characterization

Single crystal XRD data reported in the following tables come from two different single crystal samples. The two different samples were synthesized at high pressure high temperature (4 GPa and 1500 K) using multi-anvil presses. Boron atoms substitute silicon only inside the 8c Wyckoff site. Including additional boron substitutional sites in the structural refinement produced no meaningful changes to the fit and these results are, therefore, not reported (See Tables C and C).

	Crystal n°1	Crystal n°2
Composition	$\text{Na}_{8(1)}\text{B}_{4.1(2)}\text{Si}_{41.9(2)}$	$\text{Na}_8\text{B}_{4.51(10)}\text{Si}_{41.49(10)}$
Formula weight (kg.mol^{-1})	1405.04	1397.9
Temperature (K)	293	293
Crystal system	Cubic	Cubic
Space group	$I\bar{4}3m$	$I\bar{4}3m$
Lattice parameter (\AA)	9.69910(10)	9.6794(4)
Volume (\AA^3)	912.42(3)	906.87(6)
Wavelength (\AA)	0.7107	0.4066
Diffractometer	RIGAKU (Agilent) Xcalibur S	APS, HPCAT
Number of refined reflections	280	141
h, k, l index range	$-13 \leq h \leq 13$; $-13 \leq k \leq 13$; $-13 \leq l \leq 12$	$-12 \leq h \leq 11$; $-11 \leq k \leq 12$; $-7 \leq l \leq 4$
Goodness of fit	1.241	4.81
Final R indexes ($I > 3\sigma(I)$)	$R(F^2) = 0.0438$, $wR(F^2) = 0.1073$	$R(F^2) = 0.0599$, $wR(F^2) = 0.0740$
Software for refinement	Olex2, Shelx	Olex2, Shelx

TABLE II. Type-VIII $\text{Na}_8\text{B}_{4.1(2)}\text{Si}_{41.9(2)}$ and type VIII $\text{Na}_8\text{B}_{4.51(10)}\text{Si}_{41.49(10)}$ experimental crystallographic data processing.

Atom	Site	x	y	z	B (temp)	Occupancy
Na1	8c	0.6882(2)	0.6882(2)	0.6882(2)	1.0106	1
Si1	12d	0.25	0.5	0	0.1921	1
Si2	2a	0	0	0	0.4974	1
Si3	24g	0.08527(17)	0.08527(13)	0.65559(13)	0.3606	1
Si4/B	8c	0.8654(2)	0.8654(2)	0.8654(2)	0.5922	0.49(2) (Si) 0.51(2) (B)

TABLE III. Experimental structure data of $\text{Na}_8\text{B}_{4.1(2)}\text{Si}_{41.9(2)}$ type-VIII clathrate. The associated anisotropic displacement tensors U_{ij} are:

Na1 : $U_{11} = U_{22} = U_{33} = 0.0128(9)$; $U_{23} = U_{13} = U_{12} = 0.0046(9)$
Si1 : $U_{11} = U_{22} = U_{33} = 0.0075(13)$; $U_{23} = U_{13} = U_{12} = 0.0030(8)$
Si2 : $U_{11} = U_{22} = U_{33} = 0.0063(9)$; $U_{23} = U_{13} = U_{12} = 0$
Si3 : $U_{11} = 0.0101(8)$; $U_{22} = U_{33} = 0.0018(5)$; $U_{23} = 0.0013(5)$; $U_{13} = U_{12} = 0.0018(3)$
Si4/B : $U_{11} = U_{33} = 0.0161(4)$; $U_{22} = 0.0037(8)$; $U_{23} = U_{13} = U_{12} = 0$

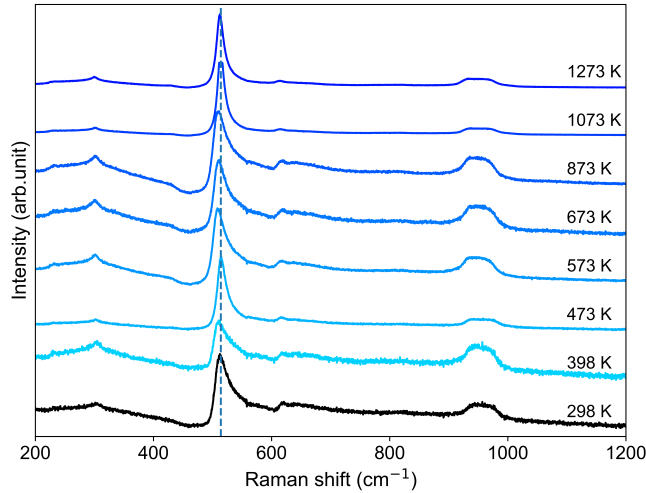


FIG. 9. Raman spectrum of $\text{Na}_8\text{B}_{4.51}\text{Si}_{41.49}$ type-VIII single-crystal clathrate after annealing at high temperature.

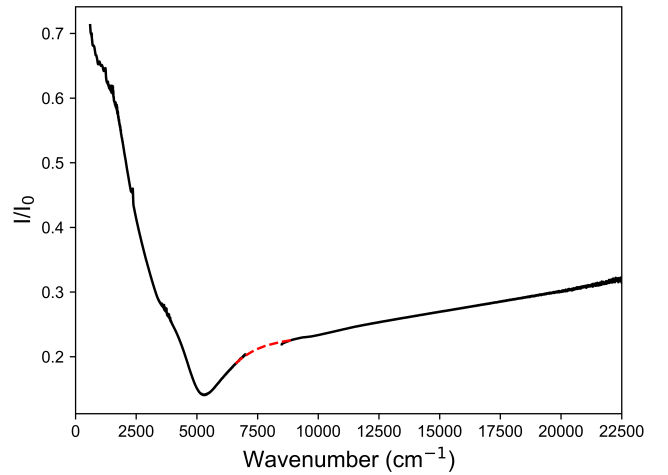


FIG. 10. Reflectance FTIR spectroscopy at ambient condition of $\text{Na}_8\text{B}_{4.51}\text{Si}_{41.49}$ type-VIII single-crystal clathrate.

Atom	Site	x	y	z	B (temp)	Occupancy
Na1	8c	0.18798(14)	0.18798(14)	0.18798(14)	0.0229(5)	1
Si1	12d	0.25	0.5	0	0.0161(4)	1
Si2	2a	0	0	0	0.0115(2)	1
Si3	24g	0.41438(6)	0.41438(6)	0.15688(8)	0.0133(19)	1
Si4/B	8c	0.52294(13)	0.52294(13)	0.52294(13)	0.0154(6)	0.436(12) (Si) 0.564(12) (B)

TABLE IV. Experimental structure data of $\text{Na}_8\text{B}_{4.51(10)}\text{Si}_{41.49(10)}$ type-VIII clathrate. The associated anisotropic displacement tensors U_{ij} are:

Na1 : $U_{11} = U_{22} = U_{33} = 0.0229(5)$; $U_{23} = U_{13} = U_{12} = -0.0037(5)$

Si1 : $U_{11} = U_{22} = U_{33} = 0.0161(4)$; $U_{23} = U_{13} = U_{12} = 0$

Si2 : $U_{11} = 0.0120(3)$; $U_{22} = U_{33} = 0.0112(3)$; $U_{23} = U_{13} = U_{12} = 0$

Si3 : $U_{11} = U_{22} = 0.0106(2)$; $U_{33} = 0.0187(3)$; $U_{23} = U_{13} = 0.00213(16)$; $U_{12} = 0.0012(2)$

Si4/B : $U_{11} = U_{22} = U_{33} = 0.0154(6)$; $U_{23} = U_{13} = U_{12} = -0.0026(4)$

The FTIR reflectance spectrum exhibits a trend similar to that of typical metals (Al, Ag, Au) [23] as well as to that of the BC8-Si (Si-III) phase, which is classified as a narrow-gap semiconductor [24]. The $\text{Na}_8\text{B}_{4.51}\text{Si}_{41.49}$ type-VIII single-crystal clathrate shows a reflectance minimum at 5295 cm^{-1} , where the I/I_0 ratio drops to 0.14. This minimum corresponds to an absorption energy of 0.66 eV, which lies between the absorption energies of

BC8-Si (0.16 eV) and of the other metals ($> 2\text{ eV}$). Additional resistivity measurements are therefore required to confirm the metallicity of this phase, while the hypothesis of a narrow-gap semiconductor is not entirely excluded.

REFERENCES

- [1] R. Himeno, T. Kume, F. Ohashi, T. Ban, and S. Nonomura, Optical absorption properties of na₈si₁₃₆ clathrate studied by diffuse reflection spectroscopy, *Journal of Alloys and Compounds* **574**, 398 (2013).
- [2] Y. He, F. Sui, S. M. Kauzlarich, and G. Galli, Si-based earth abundant clathrates for solar energy conversion, *Energy Environ. Sci.* **7**, 2598 (2014).
- [3] H. Kawaji, H.-o. Horie, S. Yamanaka, and M. Ishikawa, Superconductivity in the silicon clathrate compound (na,ba)₈si₄₆, *Physical Review Letters* **74**, 1427 (1995).
- [4] A. Dopilka, J. M. Weller, A. Ovchinnikov, A. Childs, S. Bobev, X. Peng, and C. K. Chan, Structural origin of reversible li insertion in guest-free, type-II silicon clathrates, *Advanced Energy and Sustainability Research* **2**, 2000114 (2021).
- [5] D. Neiner, N. L. Okamoto, P. Yu, S. Leonard, C. L. Condrón, M. F. Toney, Q. M. Ramasse, N. D. Browning, and S. M. Kauzlarich, Synthesis and characterization of $\text{K}_{2-x}\text{Hf}_2\text{Si}_{46}$, *Inorganic Chemistry* **49**, 815 (2010).
- [6] J.-A. Dolyniuk, B. Owens-Baird, J. Wang, J. V. Zaikina, and K. Kovnir, Clathrate thermoelectrics, *Materials Science and Engineering: R: Reports* **108**, 1 (2016).
- [7] A. V. Shevelkov and K. Kovnir, Zintl clathrates, in *Zintl Phases: Principles and Recent Developments*, edited by T. F. Fässler (Springer, Berlin, Heidelberg, 2011) pp. 97–142.
- [8] S. Leoni, W. Carrillo-Cabrera, and Y. Grin, Modelling of the a (clathrate VIII) to b (clathrate I) phase transition in $\text{eu}_8\text{ga}_{16}\text{ge}_{30}$, *Journal of Alloys and Compounds* (2003).
- [9] J.-M. Hübner, W. Carrillo-Cabrera, P. Kozelj, Y. Prots, M. Baitinger, U. Schwarz, and W. Jung, A borosilicide with clathrate VIII structure, *Journal of the American Chemical Society* **144**, 13456 (2022).
- [10] W. Jung, J. Lörincz, R. Ramlau, H. Borrmann, Y. Prots, F. Haarmann, W. Schnelle, U. Burkhardt, M. Baitinger, and Y. Grin, $\text{K}_7\text{B}_7\text{Si}_{39}$, a borosilicide with the clathrate I structure, *Angewandte Chemie International Edition* **46**, 6725 (2007).
- [11] J.-M. Hübner, W. Jung, M. Schmidt, M. Bobnar, P. Kozelj, B. Böhme, M. Baitinger, M. Etter, Y. Grin, and U. Schwarz, Cage adaption by high-pressure synthesis: The clathrate-I borosilicide $\text{rb}_8\text{b}_8\text{si}_{38}$, *Inorganic Chemistry* **60**, 2160 (2021), publisher: American Chemical Society.
- [12] J.-M. Hübner, W. Jung, P. Kozelj, M. Bobnar, R. Cardoso-Gil, U. Burkhardt, B. Böhme, M. Baitinger, U. Schwarz, and Y. Grin, Mastering extreme size constraints in the clathrate-I borosilicide $\text{cs}_8\text{b}_8\text{si}_{38}$, *Zeitschrift für anorganische und allgemeine Chemie* **647**, 119 (2021).
- [13] Y. Song, I. Gómez-Recio, R. Kumar, C. Coelho Diogo, S. Casale, I. Génois, and D. Portehault, A straightforward approach to high purity sodium silicide na_4si_4 , *Dalton Transactions* **50**, 16703 (2021).
- [14] P. Vinet, J. Ferrante, J. H. Rose, and J. R. Smith, Compressibility of solids, *Journal of Geophysical Research: Solid Earth* **92**, 9319 (1987).
- [15] O. O. Kurakevych, T. A. Strobel, D. Y. Kim, T. Muramatsu, and V. V. Struzhkin, Na-si clathrates are high-pressure phases: A melt-based route to control stoichiometry and properties, *Crystal Growth & Design* **13**, 303 (2013).
- [16] S. Yamanaka, M. Komatsu, M. Tanaka, H. Sawa, and

- K. Inumaru, High-pressure synthesis and structural characterization of the type II clathrate compound $\text{Na}_{30.5}\text{Si}_{136}$ encapsulating two sodium atoms in the same silicon polyhedral cages, *Journal of the American Chemical Society* **136**, 7717 (2014).
- [17] M. Gerin, D. Machon, S. Radescu, S. Le Floch, Y. Le Godec, T. Gaudisson, F. Alabarse, P. Veber, R. Debord, D. Amans, and V. Pischedda, Structural transitions at high pressure and metastable phase in $\text{Si}_{0.8}\text{Ge}_{0.2}$, *Journal of Alloys and Compounds* **954**, 170180 (2023).
- [18] Y. Zhang, Covalent radii and new applications:, *International Journal of Chemoinformatics and Chemical Engineering* **7**, 42 (2018).
- [19] M. Demoucron, S. Pandolfi, Y. Guarnelli, B. Baptiste, P. Chevignon, N. Guignot, D. Portehault, T. A. Strobel, W. A. Crichton, Y. Le Godec, and A. Courac, Supplementary material, isostructural phase transition and equation of state of type-i and type-viii metallic sodium borosilicide clathrates, *Physical Review Letters* (2025).
- [20] W. Jung, B. Böhme, J. M. Hübner, U. Burkhardt, H. Borrmann, M. Bobnar, H. D. Nguyen, I. Pantenburg, M. Etter, U. Schwarz, Y. Grin, and M. Baitinger, The impact of boron atoms on clathrate-i silicides: composition range of the borosilicide $\text{K}_{8-x}\text{Si}_{46-y}$, *Dalton Transactions* **50**, 1274 (2021).
- [21] R. Kumar and M. Tanwar, Effect of some physical perturbations and their interplay on raman spectral line shapes in silicon: A brief review, *Journal of Raman Spectroscopy* **52**, 2100 (2021).
- [22] C. Rani and R. Kumar, Fano-type discrete-continuum interaction in perovskites and its manifestation in raman spectral line shapes, *Chemical Communications* **60**, 2115 (2024).
- [23] K. Shanks, S. Senthilarasu, and T. K. Mallick, Optics for concentrating photovoltaics: Trends, limits and opportunities for materials and design, *Renewable and Sustainable Energy Reviews* **60**, 394 (2016).
- [24] H. Zhang, H. Liu, K. Wei, O. O. Kurakevych, Y. Le Godec, Z. Liu, J. Martin, M. Guerrette, G. S. Nolas, and T. A. Strobel, Be_8 silicon (si-iii) is a narrow-gap semiconductor, *Physical Review Letters* **118**, 146601 (2017), publisher: American Physical Society.
- [25] R. Nesper, The zintl-klemm concept – a historical survey, *Zeitschrift für anorganische und allgemeine Chemie* **640**, 2639 (2014).
- [26] L. Vegard, Die konstitution der mischkristalle und die raumfüllung der atome, *Zeitschrift für Physik* **5**, 17 (1921).
- [27] O. L. Anderson, D. G. Isaak, and S. Yamamoto, Anharmonicity and the equation of state for gold, *Journal of Applied Physics* **65**, 1534 (1989).
- [28] L. Lutterotti, Maud : Materials analysis using diffraction (2025).
- [29] S. Anzellini, M. T. Wharmby, F. Miozzi, A. Kleppe, D. Daisenberger, and H. Wilhelm, Quasi-hydrostatic equation of state of silicon up to 1 megabar at ambient temperature, *Scientific Reports* **9**, 15537 (2019).
- [30] A. Dewaele, F. Datchi, P. Loubeyre, and M. Mezouar, High pressure-high temperature equations of state of neon and diamond, *Physical Review B* **77**, 094106 (2008).
- [31] A. Dewaele, A. D. Rosa, N. Guignot, D. Andrault, J. E. F. S. Rodrigues, and G. Garbarino, Stability and equation of state of face-centered cubic and hexagonal close packed phases of argon under pressure, *Scientific Reports* **11**, 15192 (2021).
- [32] R. Debord, H. Euchner, V. Pischedda, M. Hanfland, A. San-Miguel, P. Mélinon, S. Pailhès, and D. Machon, Isostructural phase transition by point defect reorganization in the binary type-i clathrate $\text{Ba}_{7.5}\text{Si}_{45}$, *Acta Materialia* **210**, 116824 (2021).
- [33] A. San-Miguel, P. Mélinon, D. Connétable, X. Blase, F. Tournus, E. Reny, S. Yamanaka, and J. P. Itié, Pressure stability and low compressibility of intercalated cage-like materials: The case of silicon clathrates, *Physical Review B* **65**, 054109 (2002).
- [34] A. S. Miguel, A. Merlen, P. Toulemonde, T. Kume, S. L. Floch, A. Aouizerat, S. Pascarelli, G. Aquilanti, O. Mathon, T. L. Bihan, J.-P. Itié, and S. Yamanaka, Pressure-induced homothetic volume collapse in silicon clathrates, *Europhysics Letters (EPL)* **69**, 556 (2005).
- [35] P. Toulemonde, D. Machon, A. San Miguel, and M. Amboage, High pressure x-ray diffraction study of the volume collapse in $\text{Ba}_{24}\text{Si}_{100}$ clathrate, *Physical Review B* **83**, 134110 (2011).
- [36] T. Itaka, Pressure-induced isostructural phase transition of metal-doped silicon clathrates, *Physical Review B* **75**, 012106 (2007).
- [37] J. Gonzalez-Platas, M. Alvaro, F. Nestola, and R. Angel, *EosFit7-GUI* : a new graphical user interface for equation of state calculations, analyses and teaching, *Journal of Applied Crystallography* **49**, 1377 (2016).
- [38] M. I. McMahon, R. J. Nelmes, N. G. Wright, and D. R. Allan, Pressure dependence of the *Imma* phase of silicon, *Physical Review B* **50**, 739 (1994).
- [39] P. Loubeyre, F. Occelli, and P. Dumas, Synchrotron infrared spectroscopic evidence of the probable transition to metal hydrogen, *Nature* **577**, 631 (2020).
- [40] M. Demoucron, Data isostructural phase transition and equation of state of type-i and -viii metallic sodium borosilicide clathrates, <https://figshare.com/account/articles/30647453> (2025).
- [41] W. A. Crichton, The EBS large-volume press facility at the ESRF, *Acta Crystallographica Section A Foundations and Advances* **80**, e415 (2024).
- [42] L. Börnstein, Numerical data and functional relationships in science and technology, group iii: crystal and solid state physics, vol. 13: Metals: phonon states, electron states and fermi surfaces, subvolume a, phonon states of elements, electron states and fermi surfaces of alloys, *Crystal Research and Technology* **17**, 326 (1982).
- [43] J. N. Fritz and B. Olinger, Equation of state of sodium, *The Journal of Chemical Physics* **80**, 2864 (1984).
- [44] J. P. Perdew and A. Zunger, Self-interaction correction to density-functional approximations for many-electron systems, *Physical Review B* **23**, 5048 (1981).
- [45] J. P. Perdew, K. Burke, and M. Ernzerhof, Generalized gradient approximation made simple, *Physical Review Letters* **77**, 3865 (1996), publisher: American Physical Society.
- [46] A. Courac, Y. Le Godec, C. Renero-Lecuna, H. Moutaabbid, R. Kumar, C. Coelho-Diogo, C. Gervais, and D. Portehault, High-pressure melting curve of zintl sodium silicide Na_4Si_4 by in situ electrical measurements, *Inorganic Chemistry* **58**, 10822 (2019).
- [47] C.-M. Sung, C. Goetze, and H.-K. Mao, Pressure distribution in the diamond anvil press and the shear strength of fayalite, *Review of Scientific Instruments* **48**, 1386

- (1977).
- [48] M. S. Anderson, R. Q. Fugate, and C. A. Swenson, Equation of state for solid neon to 20 kbar, *Journal of Low Temperature Physics* **10**, 345 (1973).
- [49] R. J. Hemley, C. S. Zha, A. P. Jephcoat, H. K. Mao, L. W. Finger, and D. E. Cox, X-ray diffraction and equation of state of solid neon to 110 GPa, *Physical Review B* **39**, 11820 (1989).